SACLANTCEN REPORT
serial no: SR- 326

SACLANT UNDERSEA RESEARCH CENTRE REPORT

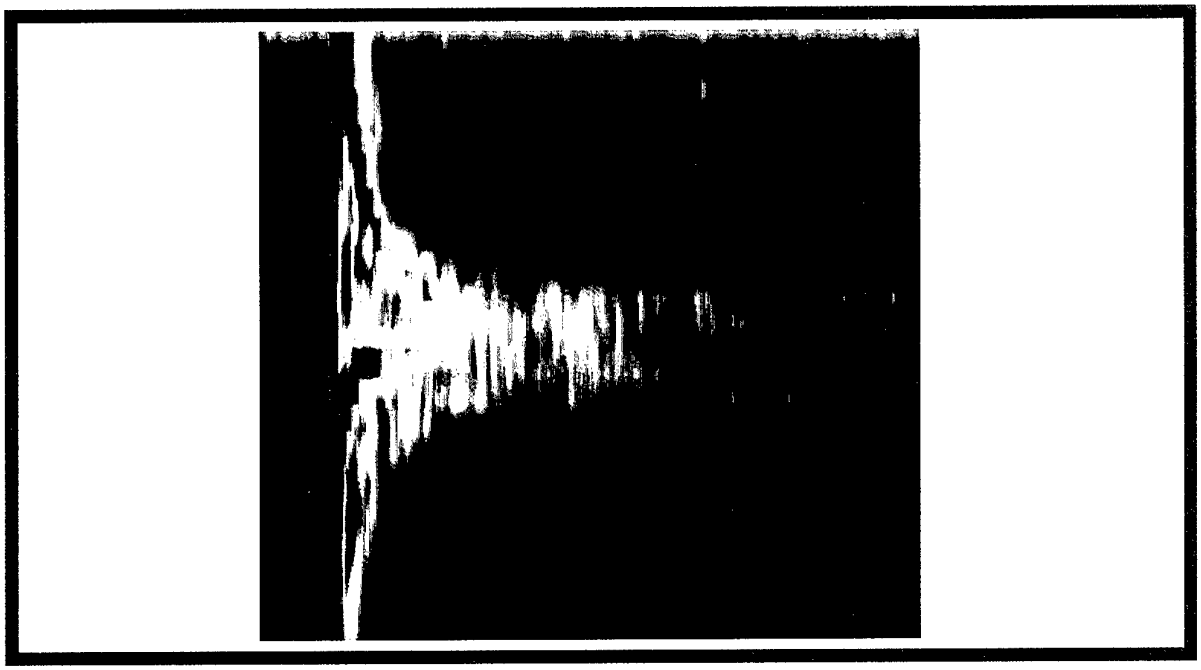

NORTH ATLANTIC TREATY ORGANIZATION ORGANISATION DU TRAITE DE L'ATLANTIQUE NORD

Shallow water reverberation from a time reversed mirror

Charles W. Holland, B. Edward McDonald

The content of this document pertains to work performed under Project 04-C of the SACLANTCEN Programme of Work. The document has been approved for release by The Director, SACLANTCEN.

Jan L. Spoelstra
Director

intentionally blank page

Shallow water reverberation from a time reversed mirror

Holland, C.W., McDonald, B.E.

Executive Summary: Reverberation arising from a time-reversed signal has a peculiar feature, which may be exploited for military or scientific applications. The peculiarity is that at the same range of the focus, there is a potential decrease in reverberation from the ocean boundaries. The significance of this effect is the potential gain in signal-to-reverberation for active sonar systems operating against targets in shallow water, where reverberation from the bottom boundary is often the limiting factor in system performance.

In this report, 3500 Hz reverberation measurements and modeling from a time-reversed signal are presented to examine the potential reverberation reduction at the target range offered by such a system. Results indicate that in order to exploit the bottom reverberation reduction, substantial azimuthal resolution may be required. The amount of horizontal resolution needed is proportional to the severity of the environmental range dependence around the target. Modeling results showed that even small bathymetric variations can lead to a significant loss of gain against reverberation.

Measurements and modeling are also presented for a potential scientific measurement where seafloor reverberation is enhanced at the focal range. This is done by focusing at the seafloor, which provides a unique opportunity to measure long-range bottom scattering by eliminating scattering contributions from the water column or sea-surface. Focusing at the seafloor was experimentally observed with an omnidirectional receiver, which is promising for using time-reversal as scientific tool for long range scattering measurements. However, quantitative results require a receiver with horizontal directionality.

The analysis results reported here gave birth to several new ideas to be pursued in the future. We propose that the azimuthal width of the focal region could be probed by measurement of the horizontal directionality of the reverberation. This would allow an extremely rapid and simple monitoring technique. The second idea is based on the extreme sensitivity of the reverberation to bathymetric features. We propose that this sensitivity could potentially be exploited to remotely measure the bathymetry.

intentionally blank page

Shallow water reverberation from a time reversed mirror

Holland, C.W., McDonald, B.E.

Abstract: Modelling indicates that when the ocean boundaries are the dominant cause of reverberation, the signal-to-reverberation ratio at a target will be increased by generating a time-reversed signal from a vertical array. This occurs because the focusing 1) increases the signal level at the target and 2) reduces the boundary illumination (hence reverberation). An experiment (as part of FAF99) was designed to study the latter (i.e., potential gain against reverberation) resulting from a 3.5 kHz time-reversed signal. Results show the extreme sensitivity of the gain to bathymetric variation and indicate the need for potentially high horizontal spatial resolution in the receive array to exploit this gain.

Keywords:

Contents

1
Introduction

The ability to re-focus energy using a time reversed mirror in the ocean has been experimentally demonstrated by Kuperman *et al.* (1998) [other useful references include Hodgkiss *et al.* (1999) and Song *et al.* (1999)]. The feature of interest in these experiments has been the characteristics of the focal spot. Another potentially useful aspect of the time-reversed mirror concept is the resultant reverberation. Exploring the reverberation has at least two important aspects. First, the reverberation is an important consideration for potential tactical applications since an important system metric is the target illumination-to-reverberation ratio. Second, the time-reversed mirror has the potential to be useful as a scientific tool to study shallow water bottom scattering. That is, the time reversed mirror allows one to illuminate a small region of the environment at long ranges in shallow water, which gives important potential advantages for studying bottom scattering.

Thus, the two goals of the experiment were to: 1) determine the effectiveness of the focused acoustic field (FAF) technique for reverberation reduction at 3.5 kHz and 2) examine FAF potential as research tool to measure bottom scattering. Unfortunately, equipment problems prevented the deployment of a key piece of equipment (a towed horizontal array) which prevents us from fully addressing the original objectives. The data, however, do offer the opportunity and motivation to examine some general characteristics of reverberation arising from a time-reversed signal.

In this report, the experimental method is first described along with the environmental data. The main part of the report addresses the effects of environmental variability on reverberation. Several measurements are presented along with modelling interpretations to illuminate the kinds of sensitivities that can be expected between environmental variability and reverberation from a time-reversed signal.

2
Experimental Technique

2.1 Experiment Design

Figure 1 shows the major elements of the experiment. The probe source (PS), an ITC 2001 flooded ring source, was used to transmit 2 ms and 10 ms 3500 Hz pulses across a selected path. The acoustic field from the probe source was measured using a vertical source-receive array (SRA) with inter-element spacing at 2.7 m, which then re-transmitted a time-reversed replica. The characteristics of the focused field back near the probe source was monitored by a 32-element vertical receive array (VRA) with 0.5 m inter-element spacing and a 4-element array at 2 m inter-element spacing. The reverberation resulting from the focused field was then monitored using a 32-element mid-frequency array (MFA) with 0.18 m inter-element spacing in a quasi-monostatic geometry (i.e., near the position of the SRA). The experiment plan called for the array in a horizontal configuration. Unfortunately, equipment problems rendered it impossible and instead the array was deployed vertically, as shown.

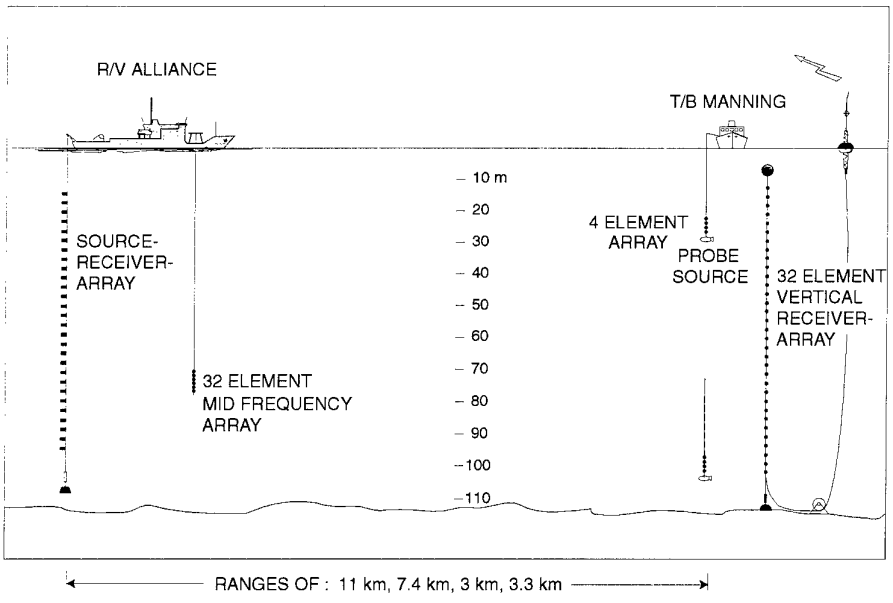

Figure 1 *FAF Reverberation Measurement Geometry*

If reverberation is dominated by boundary interaction, the time reversal process[ii] may result in a reduction of reverberation at the focal range. This is shown schematically in Fig. 2. Since the time reversal system is axisymmetric (a vertical line array) the reverberation returning at a given time comes from a spherical shell (or an annulus on the boundaries). For a probe source (PS) not on a boundary, the intensity on the boundary will be at a minimum at the same range and direction as the focal point. Thus at this time and azimuth, boundary reverberation should also be relatively small. This argument depends on the assumption that when the total intensity on the boundary is small, the incident intensity (which is responsible for the scattering/reverberation) is also small. Results presented later in this report support this assumption.

The shading of the circular annulus indicates that the boundary illumination will not be constant around the annulus if there is azimuthal anisotropy (e.g., in bathymetry, water column or sediment properties). One goal of the experiment was to determine the characteristics (depth and breadth) of the reverberation gain.

The other experimental goal was to measure the field from the converse geometry, that is when the probe source is on the boundary (for this experiment, it was the seafloor). For the converse case, under the same assumption stated above, the reverberation would be at a maximum in the source-receiver plane. It was expected that the data from this converse geometry would give clearer results inasmuch as it often experimentally easier to measure the presence, rather than the absence of a desired quantity. Nominal PS depths when it was away from the boundary were 40 m, 60 m, and 80 m. For the converse geometry, the PS depth was 1 meter above the bottom.

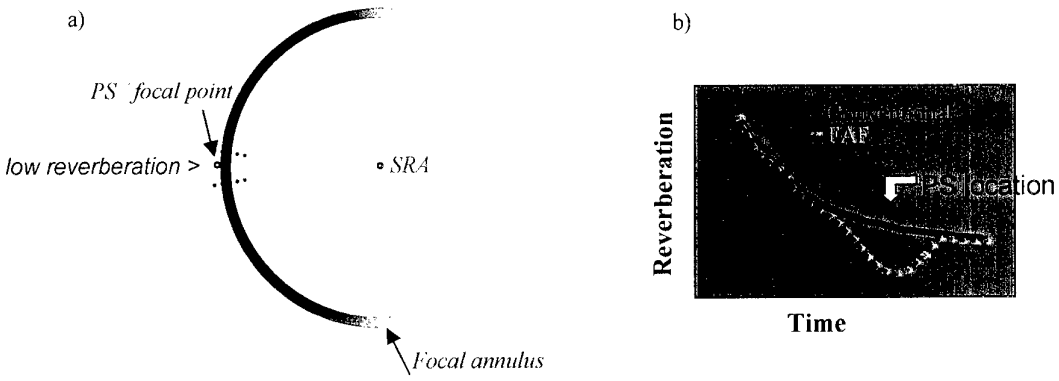

Figure 2 *Notional diagram of reverberation reduction expected from the time reversal process where the probe source is not on a boundary: a) the circular annulus represents the acoustic field on the bottom (or surface) boundary. When the probe source (PS) is not on the boundary, the total intensity on the boundary will be at a minimum at the same range and direction as the focal point. Thus at this time and azimuth boundary reverberation should also be relatively small; b) schematically shows the expected boundary reverberation from the FAF source relative to a conventional source.*

In order to examine the azimuthal behavior of the reverberation (i.e., to monitor the degradation of the focus in azimuth), the planned geometry called for the MFA to be towed perpendicular to the SRA-PS plane. Reverberation from the ambiguous beam near azimuths of the focal plane was to have been eliminated by the proximity to Formiche Island. However, equipment problems eliminated the ability to use the array in the planned horizontal configuration, and the array was instead hung in a vertical configuration as shown in Fig. 1 at a depth of about 75 m. Furthermore, the actual experiment took place in the North Elba area (see Fig. 4) rather than the planned Formiche site.

The VRA was fixed (see FVLA location on map) and the R/V *Alliance* probed the reverberation at four ranges from the VLA: 11, 3, 3.3, and 7.4 km, termed Sites 1-4 respectively. The track between the VLA and each of the four sites exhibited reasonably flat bathymetry, ranging from 112 m depth at the VLA to 118 m at the furthest site (Site 1). All of the experiments were conducted on 22 July 1999.

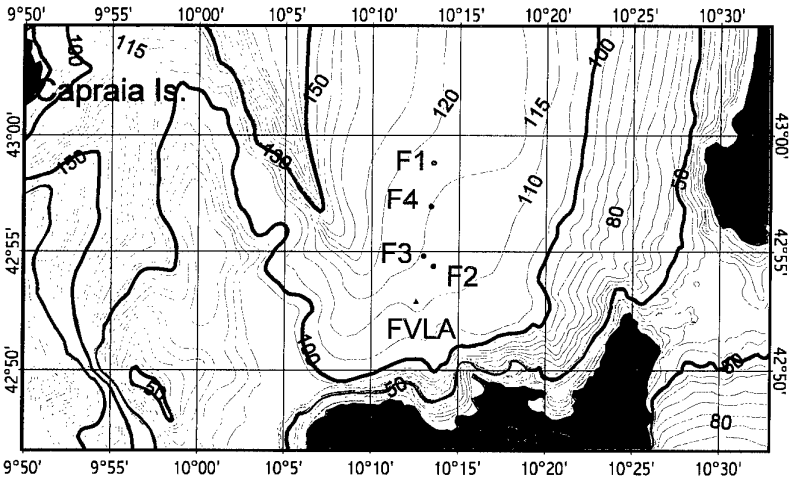

Figure 3 *Experiment Area in Capraia Basin showing the location of the vertical array (FVLA) and positions of the ALLIANCE (F1, F2, F3, and F4).*

2.2. Data Processing

Following signal conditioning, the MFA data were beamformed (Hanning shading) using a plane- wave time domain beamformer (see Sylva *et al.* (1986)) implemented in software. Beams were spaced to yield 3 dB down crossing points at 4000 Hz (see Table 1). The data were filtered in a 100 Hz band with a 6^{th} order lowpass digital elliptic filter with 0.5 dB of ripple in the passband and 50 dB of out of band rejection.

Table 1 *Receive array steer angles corresponding to beam numbers*

Beam	1	2	3	4	5	6	7	8	9	10	11	12
Angle	0.0	24.1	34.3	42.3	49.3	55.6	61.4	67.0	72.3	77.4	82.5	87.5
Beam	**13**	**14**	**15**	**16**	**17**	**18**	**19**	**20**	**21**	**22**	**23**	**24**
Angle	92.5	97.5	102.6	107.7	113.0	118.6	124.4	130.7	137.7	145.7	155.9	180

3
Environmental Data

In order to interpret the reverberation data, environmental data are required, including water column, sea surface and seafloor properties. This section provides measurements taken during this cruise and subsequent cruise named GEOSCAT99.

3.1 Water Column

The acoustic data were collected during very low wind and calm sea conditions, the sea state was 1. Figure 4 shows the sound speed measurements (from CTD casts) during the course of the day.

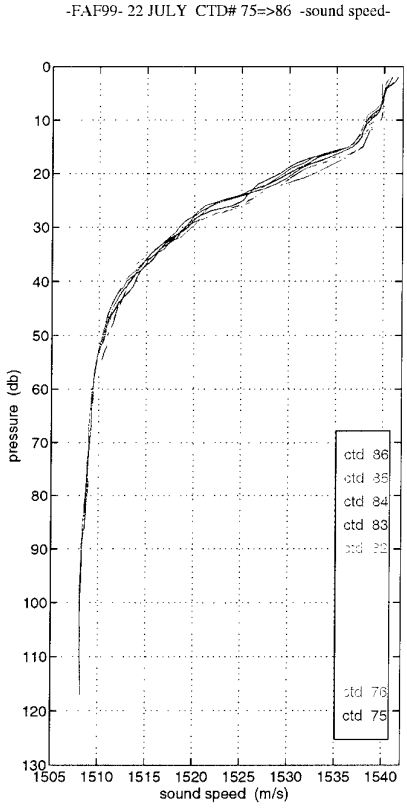

Figure 4 *Sound speed profiles taken during acoustic events from 6:40- 14:57*

3.2 Sediment Geoacoustics

Sediment geoacoustic properties (sound speed, density and attenuation) of the seafloor are required to model the reverberation. In this section, the vertical directionality of the propagation and noise data was employed to extract these properties.

3.2.1 Propagation Analysis

Figure 6 shows a 10 ms CW signal transmitted from the probe source and received on the MFA at Site 2 (about 3 km distance). The source and receiver depths were 52 m and 75 m respectively. The data have been beamformed to show the arrival structure as a function of vertical angle, with the convention that beam 1 points toward the sea surface and beam 24 towards the seafloor. The marginal plot shows the beam widths and spacing employed in the processing. The salient feature of the plot is that the arrivals are contained within a narrow angular band. This band indicates the limits of the waveguide for propagating energy. Given the bottom-limited conditions at this site, the sound speed in the seafloor is the controlling factor for those angles which do, and do not propagate. The relationship between propagating angles and the sound speed in the bottom, c_{sed}, is given simply by Snell's Law as

$$c_{sed} = c_{rec} / cos(\theta_c) \tag{1}$$

where θ_c is termed the apparent critical angle and c_{rec} is the sound speed at the receiver. In the measured data of Fig. 6 the downgoing paths are greatly attenuated for beam numbers less 9 and the upgoing paths are greatly attenuated for beam numbers greater than 15. We calculate θ_c by taking the average angle on the boundary between where the energy is visible and where it is strongly attenuated (e.g., beam 8 and 9). Thus for the downgoing and upgoing energy respectively we obtain, 20° and 15°. The asymmetry in these two angles indicates that the array may be tilted by 2.5° in the plane of the propagation. Thus, our final estimate for the apparent critical angle is 17.5°, which corresponds to a sediment sound speed of 1582 m/s.

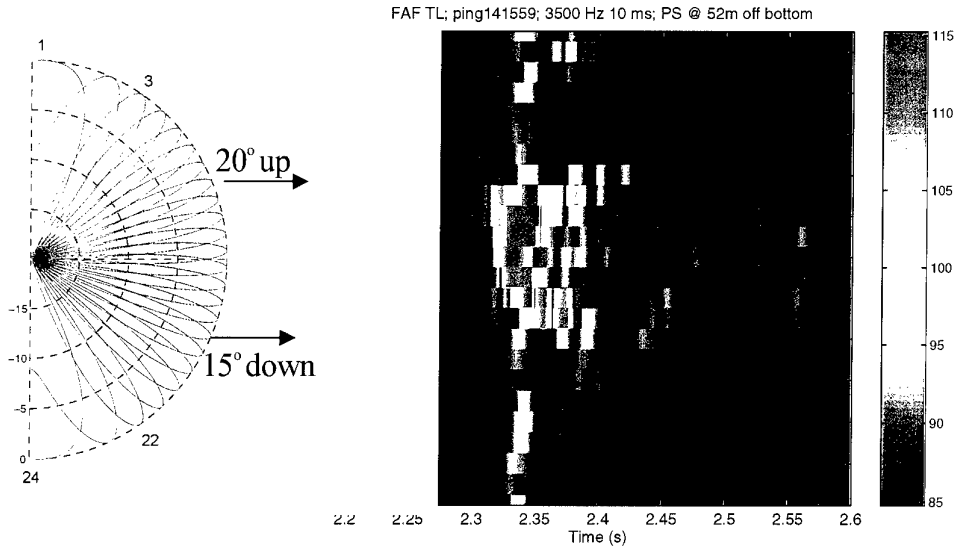

Figure 5 *One-way propagation of 10 ms CW signal from the probe source received on the MFA at Site 2; units are in dB re μPa/Hz. The marginal plot shows the analysis beampattern and numbering convention.*

3.2.2. Ambient Noise Analysis

A similar analysis can also be done for ambient noise. Figure 6 shows 1 second of 3500 Hz noise at Site 3, which seems to originate from a single large noisy ship, at an unknown but almost certainly relatively close (few km) range. No asymmetry in the upgoing versus downgoing angles is apparent which may mean that the array is straight with respect to the noise source. At this site the apparent critical angle is 15 degrees, thus the sediment sound speed from Eq. 1 is 1562 m/s.

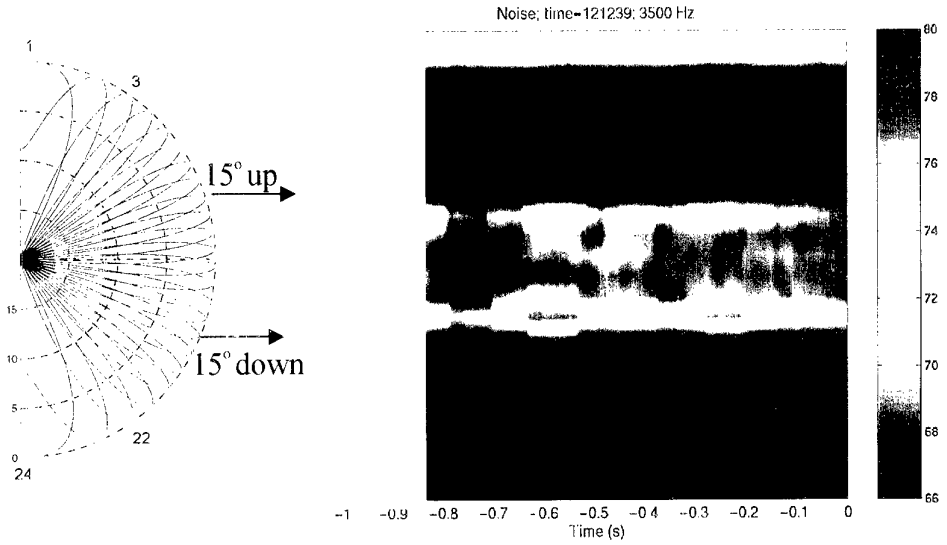

Figure 6 *3500 Hz noise sample at Site 3. The high noise from the upward looking beam is from the ALLIANCE; units are in dB re μPa/Hz. The marginal plot shows the beam pattern and beam numbering convention.*

During the GEOSCAT99 experiment, core data was taken at several of these sites and analyzed for sound speed at 50 kHz. The comparison of the halfspace inversion estimates and the core data are shown in Fig. 8. Given the low speed of the interface, the effective critical angle in the bottom is probably arises from the first sound speed maximum (at 0.12 m). From the two cores these maxima are at 1585 and 1565 which are in reasonable accordance with the critical angle estimates from the analysis above.

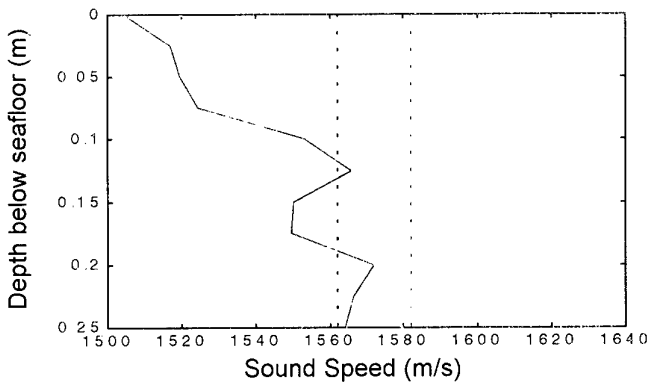

Figure 7 *Comparison of sound speed measured from core data at the VRA site (blue line) and Site F4 (green line) with the halfspace estimates from Site F2 (red dashed) and Site F3 (black dashed).*

The other geoacoustic properties (see Table 2) were obtained using empirical formulae (Hamilton (1980) and Bachman (1985)) to estimate sediment density and attenuation from the inverted sound speed.

Table 2 *Simple halfspace geoacoustic model for experiment area*

Sound speed (m/s)	1572
Density (g/cc)	1.63
Attenuation (dB/m/kHz)	.25

4

Reverberation Analysis

In this section the reverberation arising from the SRA re-transmissions and measured on the MFA are examined. First, an example of the reverberation is shown and discussed in terms of the general features. The early-time contributions from bi-static scattering are then briefly discussed. Reverberation data from a probe source placed on the bottom and in the middle of the water column are discussed in that order. The reverberation from a source placed on the boundary is expected to be, and is, easier to interpret.

Figure 9 shows an example of reverberation data from a 10 ms ping at 3500 Hz. Zero time represents the initiation of the time reversed signal from the SRA; 1 second of noise was collected before each ping. The direct blast, which overloaded the receiver, is observed across all beams shortly[iii] after the ping was transmitted. In Fig. 9, the data have been plotted against angle instead of beam number.

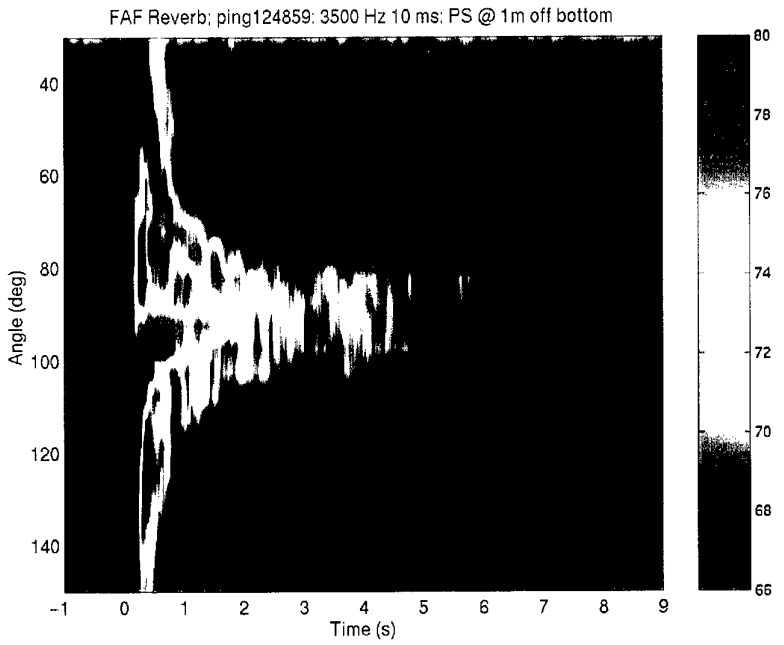

Figure 8 *Reverberation from a 10 ms 3500 Hz CW time reversed ping at Site 2; units are in dB re μPa/Hz. The initiating probe source ping was at a range of 3 km and a depth of 111 m (1 meter above the seafloor). Note the increase in reverberation at the focal range, 4 seconds.*

4.1. Bi-static scattering strength

The early time data (less than 3 seconds) show three branches. These branches correspond to three different bi-static scattering paths as shown in Figure 10.

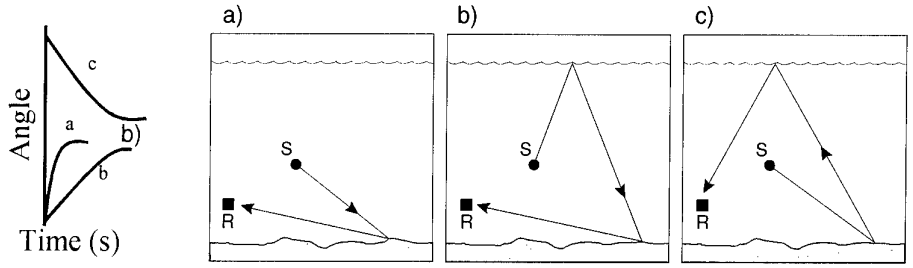

Figure 9 *Cartoon of early-time path structure from FAF reverberation geometry with ray diagram of early time bi-static scattering paths corresponding to the branches.*

A bottom scattering model has been developed (Holland *et al.* (1999)) that predicts the arrival structure as a function of time and angle as shown in Fig. 11. In this comparison, the computations were performed using only the bi-static scattering paths shown in Fig. 10. The fact that the model and data look quite similar means that the first few seconds of data are almost completely controlled by these single bounce paths. Thus the early time data could be used to analyze bi-static scattering strength near the SRA. No attempt has been made in this phase of the analysis to extract quantitative scattering strengths from the model-to-data comparisons, however, this will be pursued at a later time.

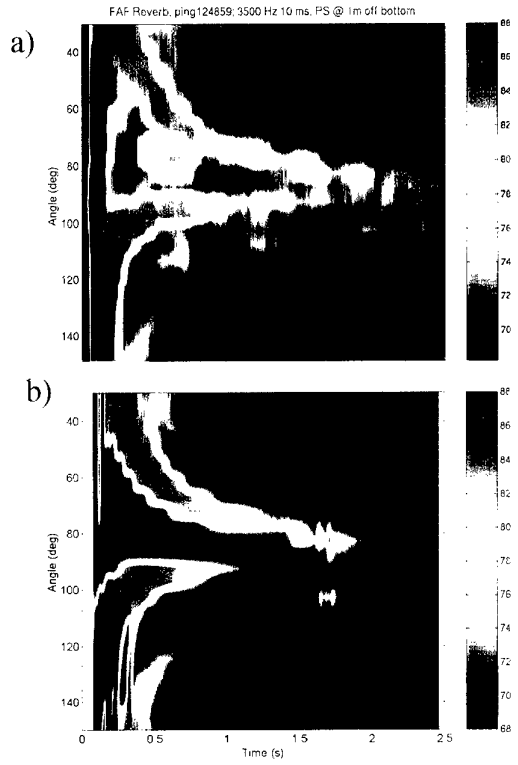

Figure 10 *Early time reverberation from a 10 ms 3500 Hz ping: a) measured and b) modelled with first-order bi-static paths only (i.e., paths shown in Figure 9).*

4.2 Probe Source and Resulting Focus on the Seafloor

In order to explore the potential for the FAF technique for measuring scattering in shallow water, the probe source was placed near (1 m above) the bottom. Figure 8 shows the resulting measured reverberation from a single 10 ms 3500 Hz ping at Site 2. The distance from the SRA to the probe source was about 3 km, which means that the reverberation from the seafloor at the focal point arrives at about 4 seconds. The increase in reverberation at 4 seconds is clearly visible. The quantitative increase in reverberation at the focal point can be observed in the data of Fig. 12a. The data are averaged using a 20 ms boxcar sliding window. The peak at the focal range is about 5 dB higher than the reverberation/noise background. Note also that there is another peak a few tenths of a second later. The reason for the existence of this second peak and the shape of both peaks will be discussed later along with discussion of Fig. 12b.

Figure 12a also contains modelled results for a an omnidirectional receiver using a combination of PROSIM [Bini-Verona (2000)] (which is based on the ORCA model [Westwood (1996)]) for the forward field (probe source to SRA) and ALMOST

[Schippers (1998)] for the reverberation component. The model used range independence in all environmental variables; the seafloor geoacoustic model was taken to be a halfspace (see Table 1). Note that in the model-to-data comparison, the modelled initial[iv] decay (first few seconds) of the reverberation matches the measurement quite well which indicates that the assumed scattering angular dependence (Lambert's Law) is reasonable in this area[v]. The scattering strength in the model was adjusted to fit the measured data.

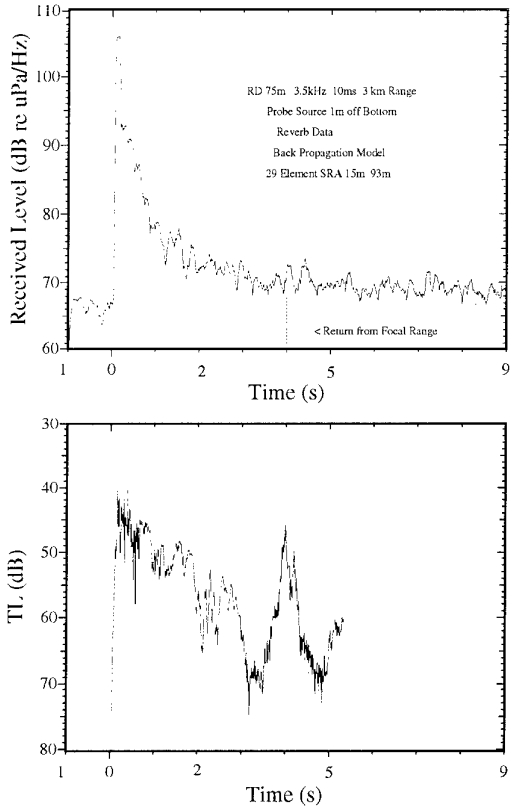

Figure 11. *a) Comparison of broadside beam data (black line) and modelled reverberation (dotted blue line) at Site 2 for a focus at the seafloor and b) modelled incident field on the bottom averaged in azimuth*

The focal annulus is an important metric when interpreting reverberation from our geometry. Figure 13 provides a cartoon of the annulus that was illuminated at the focal range for this ping. Clearly, any azimuthal anisotropy will degrade the quality of the focus (i.e., diminish the intensity of the incident field at the seafloor) and thus decrease the measured reverberation at the focal range.

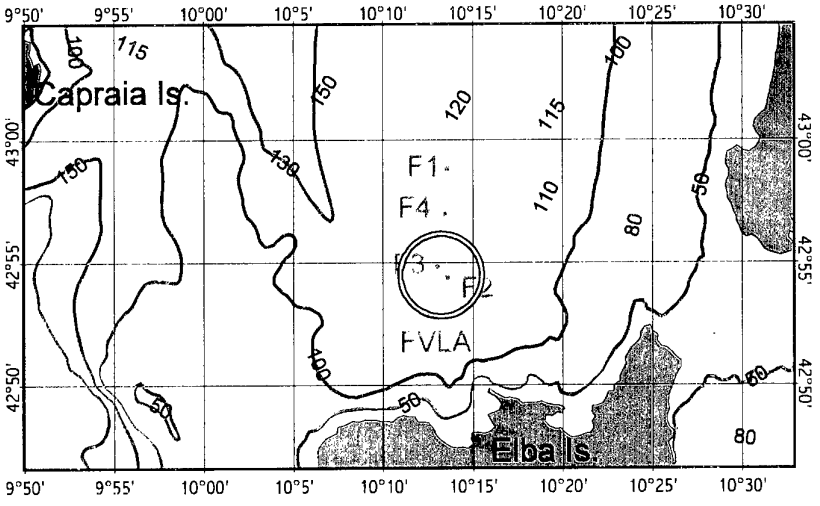

Figure 12 *Experimental area showing the focal annulus at Site 2.*

In order to quantify the possible azimuthal dependence of the focal annulus, a series of propagation calculations were made 3500 Hz. Only bathymetric range dependence is treated in the modelling. The RAM acoustic model (Collins (1993)) was chosen because of its accuracy including high propagation angles and range dependence. Time domain pulse propagation modelling has also been carried out for the end points of the forward and back propagation between the PS and SRA. The time domain modelling was performed with PROSIM. While the time domain PROSIM model results are generally consistent with experiment, the full range - depth acoustic field from RAM along the various azimuths provides better insight into the propagation physics. One can see from range - depth intensity plots the locations where the acoustic field may be intense at the ocean boundaries. Such locations are likely to be important in reverberation studies.

Numerical parameters for the modelling are as follows. The vertical grid spacing used in RAM was 5 cm, while the range step was 2 m[vi]. Comparisons (not shown here) between broadband and single frequency numerical simulations of the FAF99 SRA configuration confirm that the array element spacing of 2.7 m, while under-sampling the vertical structure of the signal from the probe source at any single frequency, was still adequate to produce a well defined focus of the broadband signal after time reversal and back propagation. Thus spatial under-sampling is compensated by bandwidth. In our results at the center frequency of 3500 Hz it was necessary to retain full 5 cm vertical resolution on the array aperture (15 – 93 m depth) to reproduce the focal structure[vii].

For the ocean environment, CTD 82 (see Fig. 5) was used to represent the water column everywhere. The water depth at the probe source was measured to be 112 m. Otherwise, bathymetry was digitized from the chart of Fig. 13 along the PS - SRA path, and along each of eight azimuths comprising the principal compass directions. Taking bathymetry values from a chart is only an approximation to reality, but it allows assessment of the likely degree of azimuthal variation in the properties of the back-propagated field. The

depth at F2 is taken to be 113 m. The forward-propagated field from PS to the SRA location F2 is shown in Fig. 14 with the source located 1 m above the bottom.

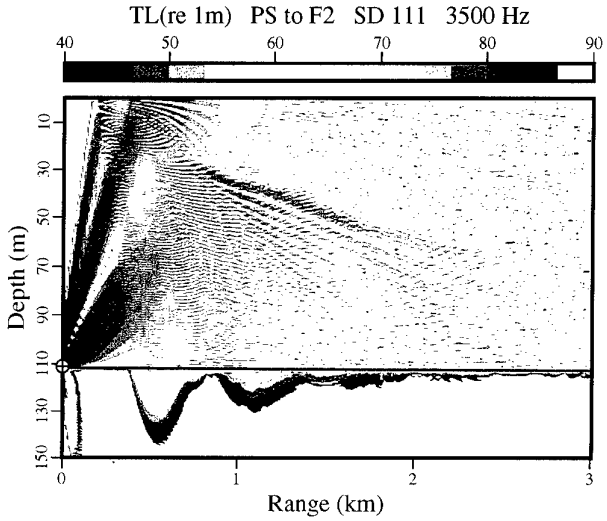

Figure 13 *Forward propagated acoustic field from FVLA to F2 with probe source one meter above the bottom.*

At site F2 the complex pressure field from the forward propagation is conjugated and projected on the array aperture spanning depths 15 to 93 m. The results for back propagation along eight azimuths are shown in Fig. 15. The layout of this figure shows the relevant bathymetry and propagation paths in the center panel. The black arrows emanating from site F2 indicate back propagation paths to seven of the eight major points of the compass (N, NE, E, SE, SW, W, and NW). For the sake of presentation clarity the southward arrow is omitted in order to show the direct path between the PS location and F2. For the seven major compass points the back propagation results are placed in their respective directions from the center panel. That is, north directly above center, east directly to the right and so on.

The green line from FVLA toward F2 in the center panel shows the forward propagation path. The back propagation result along F2 - FVLA is shown below the center panel. The focus very near the bottom at 3 km range is evident in the form of a number of convergent beams reflecting from the bottom. The low intensity in the upper water column at that range shows that a high quality focus is achieved. One might assign a 3 dB vertical width of the focal spot on the order of 2 m, and a horizontal width of order 100 m. One sees also a nearly symmetric acoustic field on either side of the focal region

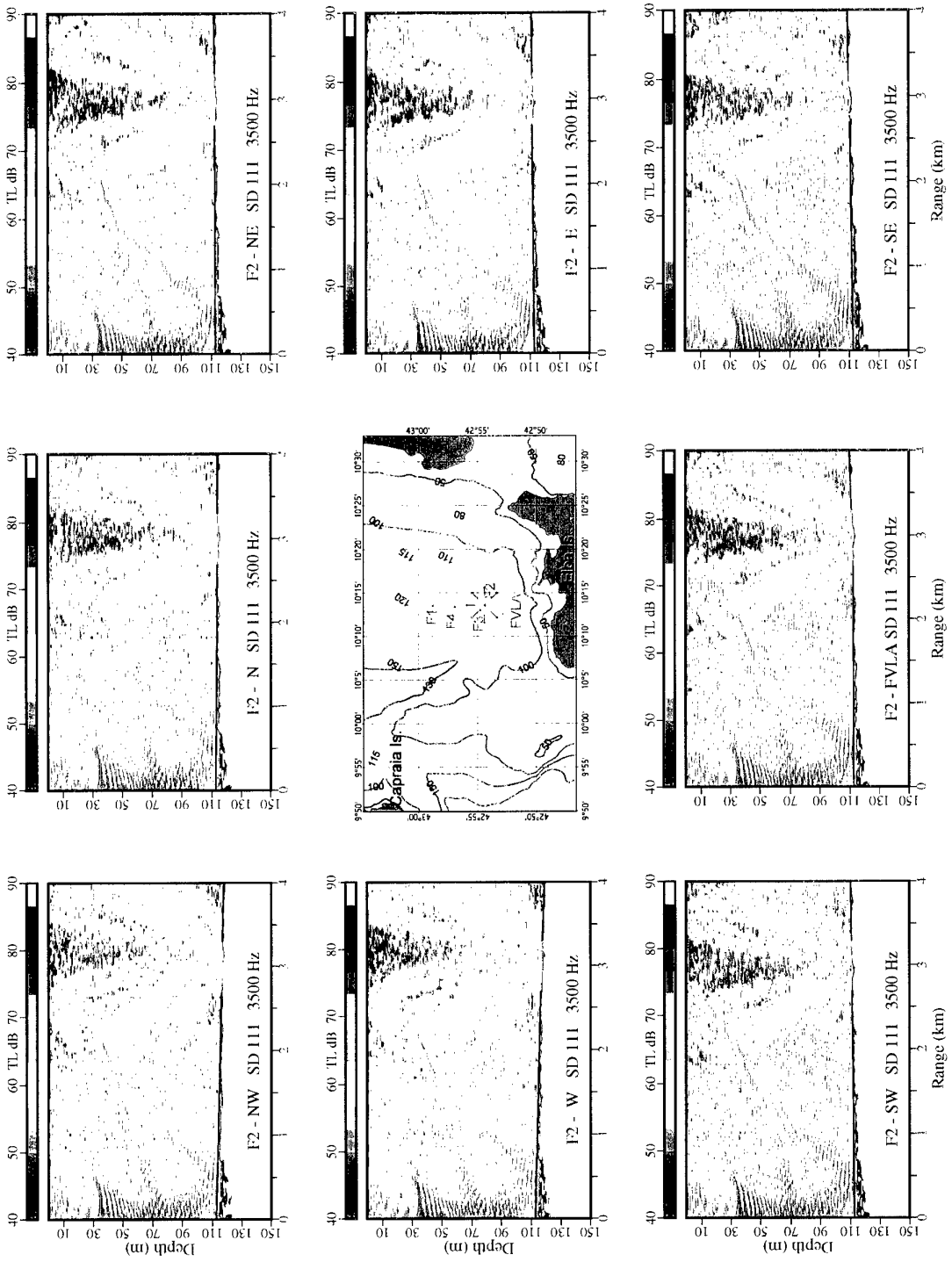

Figure 14 *Back propagated acoustic fields from F2 to seven azimuths along principal compass directions plus the path F2 - FVLA (bottom center panel) back to the probe source location. The Center panel gives the bathymetry and the back propagation azimuths as black or green lines.*

with a path of maximum intensity revealing the first one and one half cycle distances resulting from the downward refracting SSP. The familiar cycling behavior becomes visible after high propagation angle energy is lost to the bottom.

Differences among the back propagation TL results in Fig. 15 arise from differences in bathymetry along the various back propagation paths. Since the 3 km back propagation range is small and the bathymetry variation mild, one could approximate the bathymetry along a given track by a straight line between the endpoint depths. Thus it is possible to associate the various back propagation TL results with their average slope relative to that along the path F2 - FVLA. The relative slopes for the back propagation paths are shown in Table 3

Path	Depth at 3.0 km Range(m)	Relative Slope(deg)	Focal Shift(m)	Relative Reverb(dB)
F2 – FVLA	112.0	0.0	0	0
F2 – SW	111.0	0.019	-24	-13
F2 – W	117.0	-0.095	144	-44
F2 – NW	116.7	-0.090	144	-43
F2 – N	114.1	-0.040	64	-29
F2 – NE	112.2	-0.004	16	-5
F2 – E	111.2	0.015	-24	-8
F2 - SE	109.8	0.042	-56	-23

Table 3 *summarizes the back propagation results in Figure 14 and the incident transmission loss at the bottom of Fig. 15. Relative reverberation is the estimated reverberation at the focal range for various azimuths relative to that in the focal plane (F2 – FVLA path).*

In order to estimate the effect of the bathymetric variation on reverberation, the incident transmission loss at the bottom (TLin) must be calculated. This is done by decomposing the complex field produced by RAM into up and down-going waves. The intensity of the downward propagating component is averaged over an eight meter range window and expressed as incident transmission loss (TLin) relative to the probe source intensity at a distance of 1m as shown in Figure 15. From the sonar equation, reverberation is inversely proportional to 2 x TLin which assumes that scattering from all angles is the same. While this is not generally true, this assumption is considered sufficient to show how reverberation at the focus range changes in azimuth due to environmental defocusing.
From the model output used to construct the panels of Fig. 16 one can pick off the location and peak intensity of the focus on the relevant azimuths. Focal Shift in Table 3 is the range of the peak bottom insonification relative to 3.0 km. A consistent feature of the Focal Shift is that relative upslope back propagation moves the focus inward toward the SRA, while relative downslope back propagation moves it outward. The salient point is that even for these extremely small slopes, the focal spot is shifted by many pulse lengths. Thus, we can expect that a receiver with no azimuthal discrimination may have difficulty observing the reverberation peak.

The last column in Table 3, gives an indication of how the reverberation varies[viii] in azimuth at a fixed (the focal) range. It is apparent that even at this short range and nearly flat bathymetry that there is a substantial variability of the reverberation (or incident field); greater than 40 dB.

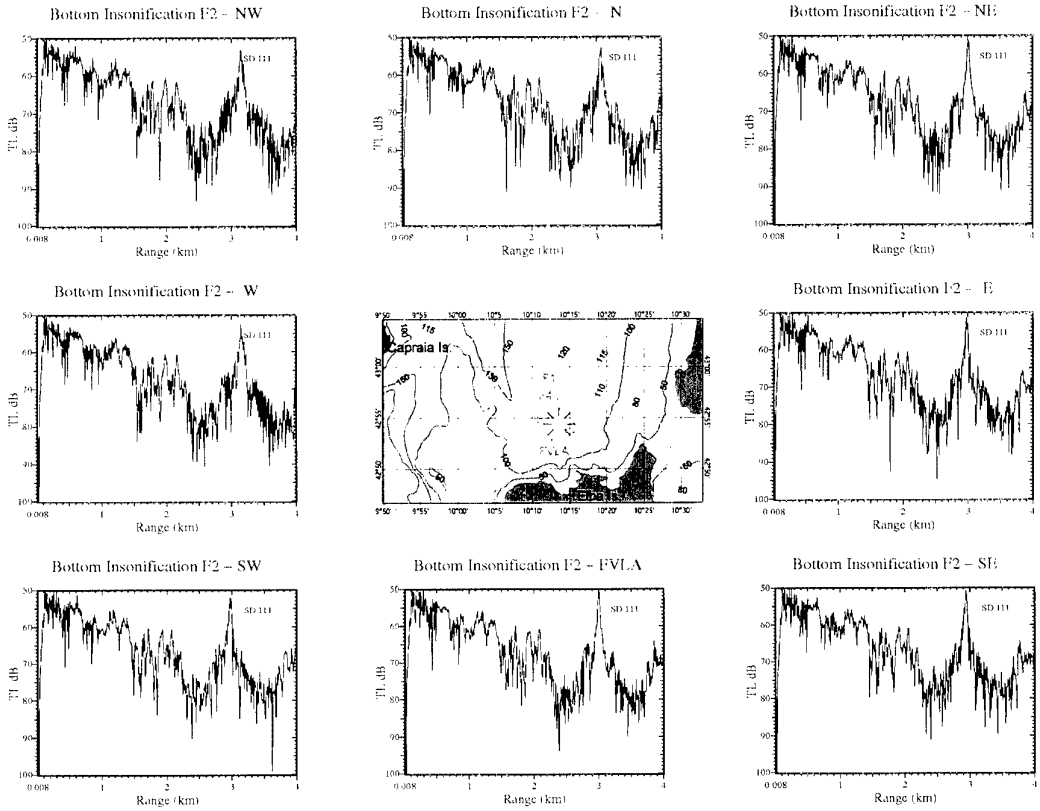

Figure 15 *Incident field on the bottom as a function of range for the eight azimuths of Fig. 14.*

Having presented the model results of ***Figure 15***, we now return to the data of Fig. 11a and the modelled incident field of Fig. 12b. Figure 12b is simply an incoherent sum (in energy) of the model results of Fig. 16; i.e., a simple averaging in azimuth of the incident field on the bottom. There are two peaks visible in the model (Fig. 11b) at about 4 seconds. The first is the main focal peak. The second peak is the focal peak from the downslope azimuths (F2-W and F2-NW). This suggests the second peak in the data of Fig. 11a is due to a focal shift caused by environmental range dependence (probably bathymetric) and that the shape of both peaks is largely due to the shape of the incident acoustic field on the seafloor. The detailed differences between model and data are likely due to the crude estimates of bathymetry that were used. Another possibility is that there is other range dependence presently unaccounted for, e.g., oceanographic or geoacoustic. However, it is our opinion that the bathymetric range dependence is the controlling factor.

In summary, the RAM model results show the relationship and extreme sensitivity between the relative bottom slope, the focal shift and resultant reverberation. In addition, the model results provide insight into the appearance of several "focal" peaks observed in the measured data.

4.3. Probe Source and Resulting Focus in Water Column

When the focus is in the water column, the bottom reverberation at the focal range should be relatively small. This is so since the incident field on the seafloor is small. Figure 16 shows measured reverberation at Site 4 from a 10 ms 3500 Hz CW ping, refocusing at a probe source depth at 60 m. At this site, the focal range is at 7.4 km (about 10 seconds) and the observed focal spot was quite sharp. However, from the data in Fig. 17, no reduction in reverberation is visible at the focal range.

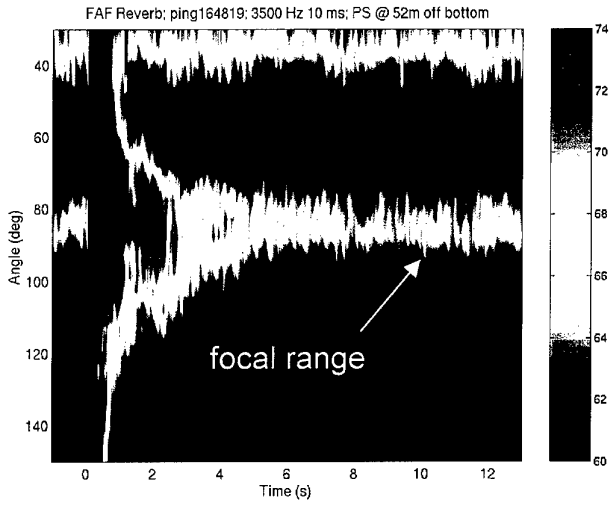

Figure 16 *Reverberation from a 10 ms 3500 Hz CW time reversed ping. The initiating probe source ping at Site 4 was at a range of 7.4 km and a depth of 60 m. For an isotropic environment we hypothesize that a reverberation reduction would be observed at the focal range, 10 seconds; however, no decrease in reverberation is observed in the data.*

Why is the reverberation reduction is not observed? Modelling results provided in the following figures indicate that the most likely cause is azimuthal anisotropy. Figure 18 shows the focal annulus superimposed on the bathymetry; the bathymetric variation around the annulus is more than 40 m (or about 30% of the water depth).

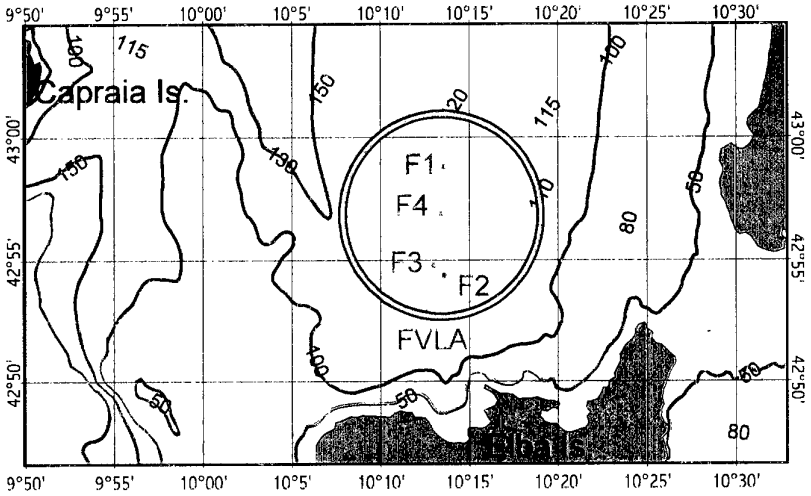

Figure 17 *Experimental area showing the focal annulus at Site 4.*

The forward acoustic fields from FVLA and the back propagated acoustic fields from the SRA at site F4 are modelled in the same manner and with the same SSP and numerical parameters as described at the end of Section B. What has changed in going to SRA at F4 is a probe source depth of 60m, a greater propagation range of 7.4 km, a 115m water depth at F4 and more variation of bathymetry along the principal azimuths. The forward propagated field from PS to the SRA location F4 is shown in Figure 19.

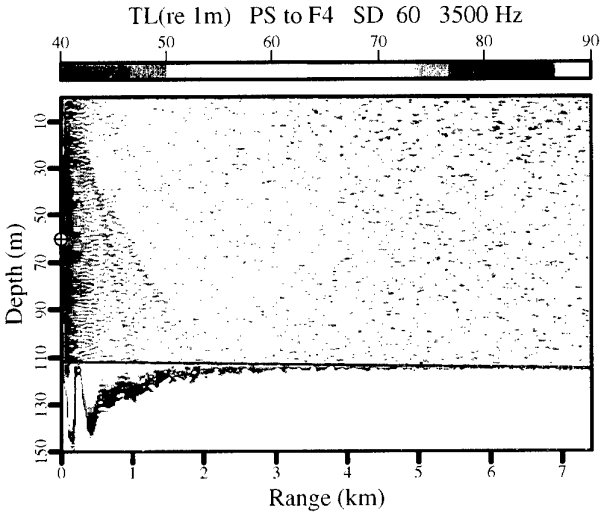

Figure 18 *Forward propagated acoustic field from FVLA to F4 with probe source at 60m depth.*

At site F4 the complex pressure field from the forward propagation is conjugated and projected on the array aperture spanning depths 15 to 93 m as in the modelling previously discussed for site F2. The results for back propagation along the eight azimuths are shown in Fig. 20. The layout of this figure is identical to that of Fig. 15. The green line in the center panel from FVLA toward F4 is the forward propagation path.

The back propagation result along F4 - FVLA is shown below the center panel. A compact focal spot at the probe source depth 60 m is evident at range 7.4 km The low intensity elsewhere in the water column at that range is evidence that a high quality focus is achieved. The vertical width of the focal spot on the order of 2 m as in the near- bottom case previously studied. The horizontal size of the spot is of order 200 m. There is again a nearly symmetric acoustic field on either side of the focal region. The cycling behavior resulting from the downward refracting SSP is also evident.

Figure 21 shows the modelled *TLin*, which can aid in the interpretation of the reverberation data. The sharp null in the incident field is readily apparent in the F4-FVLA panel at the focal range (7.4 km); however, this null, is "filled in" at most of the other azimuths[ix]. Quantitative measures of the focus and the reverberation at the focal range derived from Figs. 19 and 20 are provided in Table 4. Focal shift is determined by eye and since some of the azimuths are severely defocused one cannot determine the focal shift exactly nor to any greater accuracy than about 100 m. Note, however, that the focal shifts are significantly greater at longer ranges (compare Table 4 with Table 3) at the same relative slope.

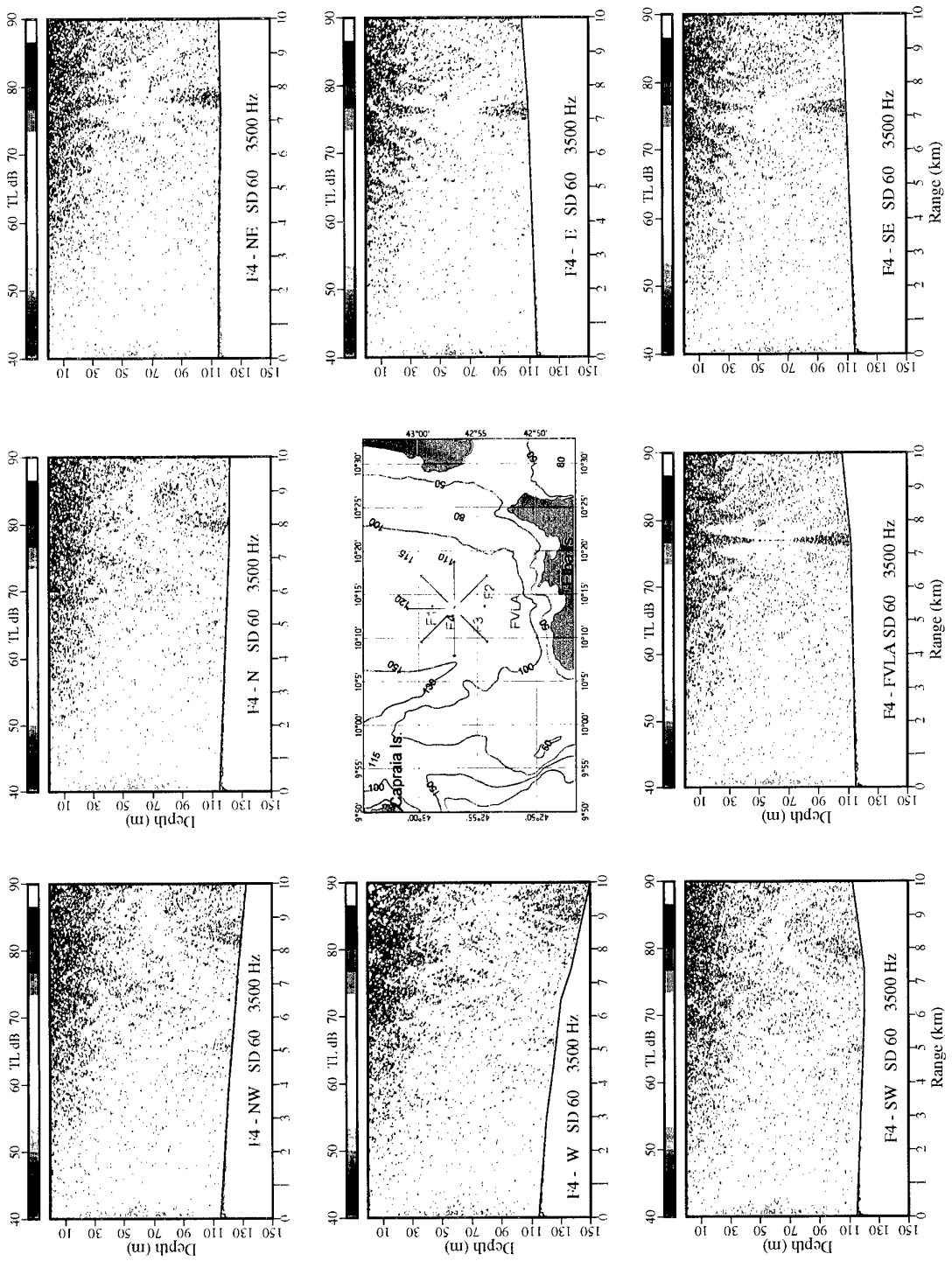

Figure 19 *Back propagated acoustic fields from F4 to seven azimuths along principal compass directions plus the path F4 - FVLA (bottom center panel) back to the probe source location. The Center panel gives the bathymetry and the back propagation azimuths as black or green lines.*

In summary, the modelling seems to support the hypothesis that no reduction in reverberation is observed because the azimuthal bathymetric variability eliminates the focus. The longer range of F4 relative to F2 results in greater azimuthal variability (for the same slope) of the focal shift and reverberation.

Path	Depth at 7.4 km Range(m)	Relative Slope(deg)	Focal Shift(m)	Relative Reverb(dB)
F4 – FVLA	112.0	0.0	0	0
F4 – SW	120.	-0.062	600	38
F4 – W	137.	-0.209	2000	35
F4 – NW	127.	-0.132	1300	39
F4 – N	121.5	-0.074	800	36
F4 – NE	116.5	-0.035	400	32
F4 – E	109	0.023	-200	28
F4 - SE	109	0.023	-200	28

Table 4 *summarizes the back propagation results in Figure 19 and the incident transmission loss at the bottom of Fig. 20. Relative reverberation is the estimated reverberation at the focal range for various azimuths relative to that in the focal plane (F4 – FVLA path).*

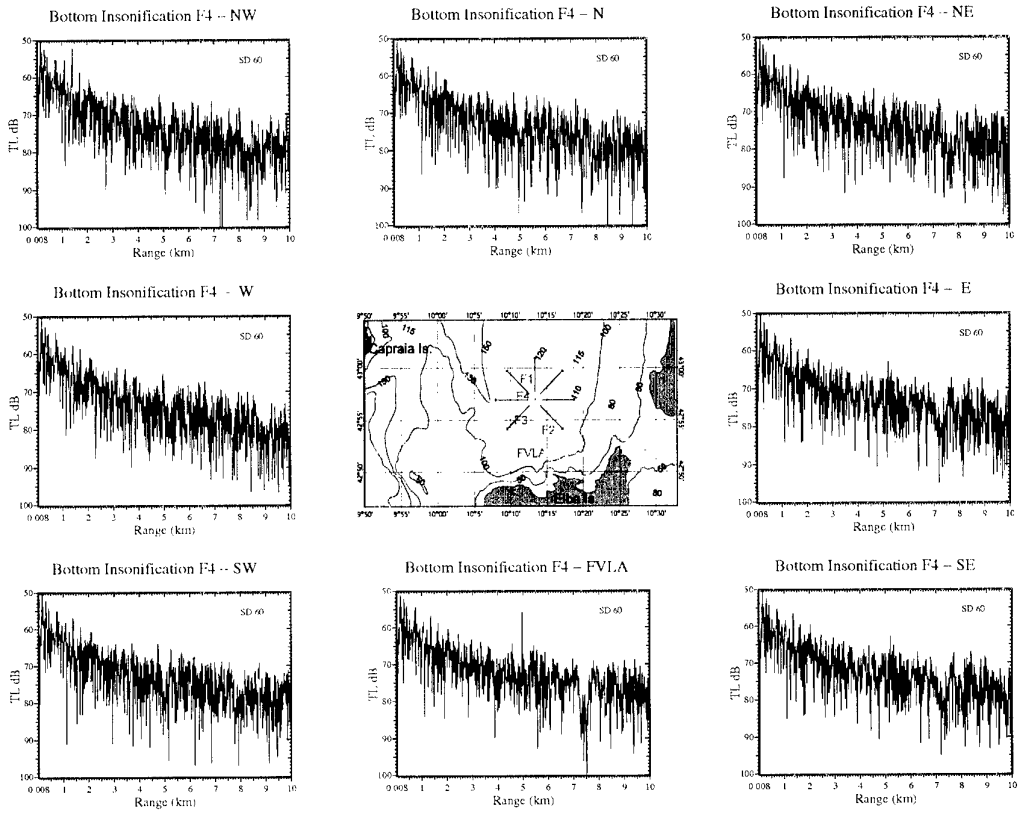

Figure 20 *Bottom insonification as a function of range for the eight azimuths of Fig.19.*

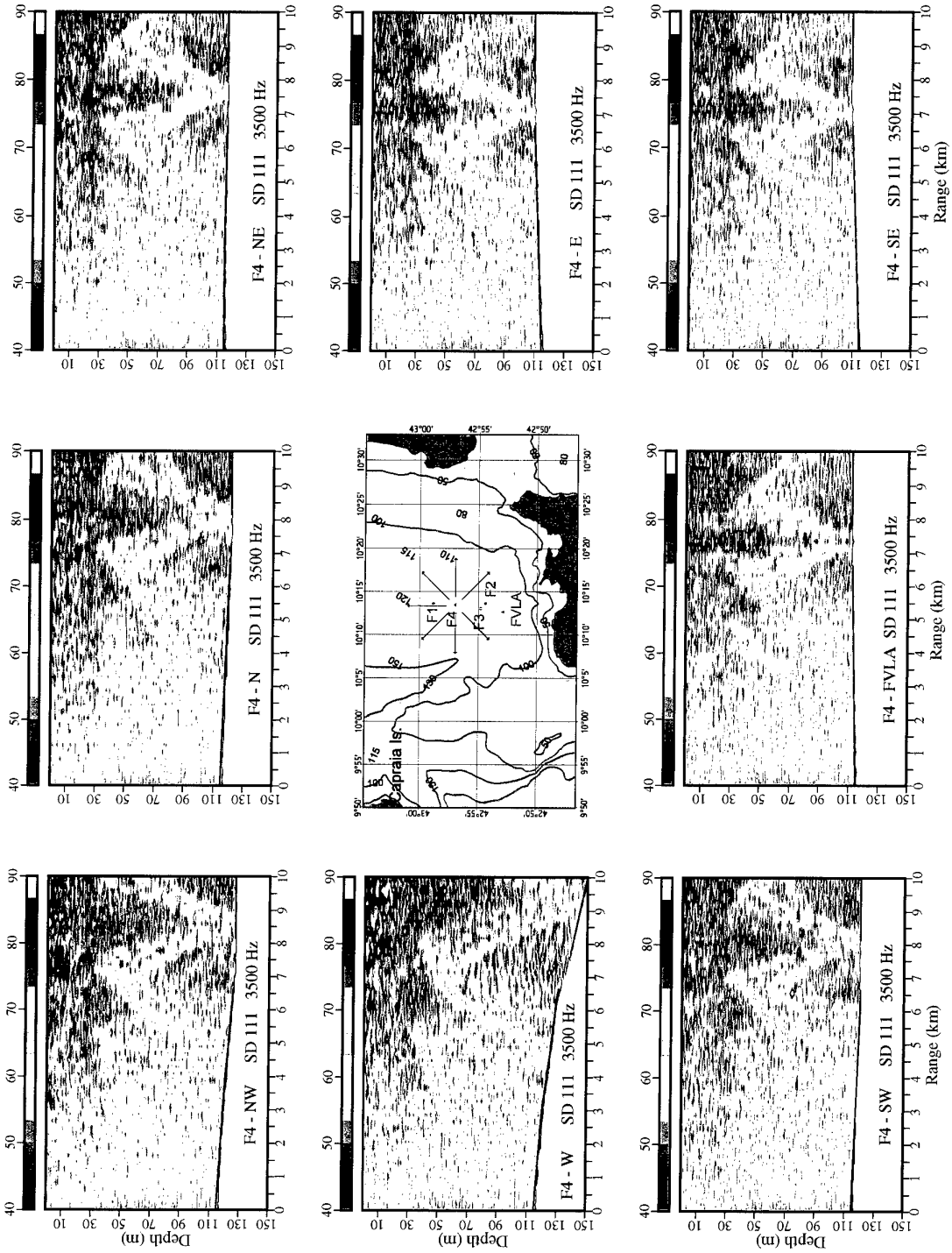

Figure 21 *Back propagated acoustic fields from F4 to azimuths along principal directions for the case of a probe source one meter above the bottom.*

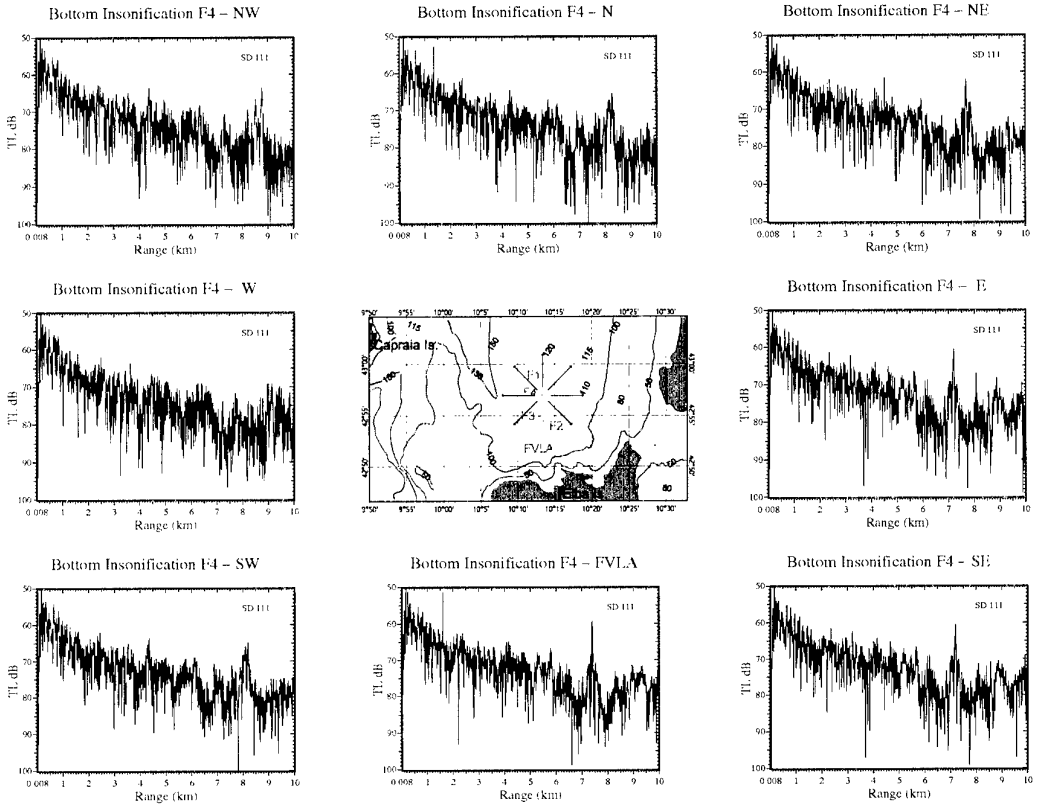

Figure 22 . *Bottom insonification as a function of range for the eight azimuths of Fig. 22.*

c	Depth at 7.4 km Range(m)	Relative Slope(deg)	Focal Shift(m)	Relative Reverb(dB)
F4 – FVLA	112.0	0.0	0	0
F4 – SW	120.	-0.062	792	-42
F4 – W	137.	-0.209	1552	-74
F4 – NW	127.	-0.132	1376	-31
F4 – N	121.5	-0.074	864	-50
F4 – NE	116.5	-0.035	288	-35
F4 – E	109	0.023	-200	-66
F4 - SE	109	0.023	-200	-66

Table 5 *summarizes the back propagation results in Figure 21 and the incident transmission loss at the bottom of Fig. 22. Relative reverberation is the estimated reverberation at the focal range for various azimuths relative to that in the focal plane (F4 – FVLA path).*

The focal shifts in Table 5 are in general agreement with those of Table 4. This example serves to indicate that the environmental anisotropy influences the focal annulus for a focal spot in the water column or on the bottom in a corresponding way.

5

Summary and Conclusions

Reverberation measurements and modeling from a focused acoustic field were presented in order to examine the potential reverberation reduction offered by focused fields. Reverberation reduction was not observed when the focus was in the water column (far from the boundaries). This result appears to be due to azimuthal anisotropy in the bathymetry. One conclusion from these results is that in order to exploit FAF for systems concepts, perhaps substantial azimuthal resolution is required. This is so, because our model results show that the gain against reverberation may take place only a very limited angular sector.

Promising results were obtained for using FAF as scientific tool for studying long range scattering in shallow water. That is, an increase in reverberation was observed when the probe source was placed close to the boundary. It was also shown that the early time reverberation is dominated by direct path bi-static scattering. Model results showed promising indications that these data can be used to extract quantitative bi-static scattering strengths. These measurements may be a valuable addition for analyzing the reverberation data.

Finally, these analyses suggested to us several new ideas. One idea is to use the horizontal directionality of the reverberation for estimating the width of the focal region. This is conceptually much easier and faster than monitoring the focal spot with a vertical array. The second idea is based on the extreme sensitivity of the reverberation to bathymetric features. We propose that this sensitivity could potentially be exploited to remotely measure the bathymetry.

Acknowledgments

We also wish to express appreciation to Tuncay Akal, test director of the FAF99 cruise. We are also indebted to Bill Kuperman, Bill Hodgkiss, and all of the science team from Scripps for many useful discussions and also for the use of their equipment. Finally, we also acknowledge and thank the captain, officers, crew and the scientific crew aboard the NRV *Alliance* (for the bottom scatter and environmental data) and RV *Manning* (for the calibration) who managed the data collection effort with adeptness.

References

Bachman, R.T., Acoustic and physical property relationships in marine sediments, *Journal of the Acoustical Society of America*, **78**, 1985:616-621.

Bini-Verona, F., Nielsen, P.L., Jensen, F.B. PROSIM broadband normal - mode model; A users' guide, SACLANTCEN SM-358.

Collins, M.D. A split-step Pad'e solution for the parabolic equation method, *Journal of the Acoustical Society of America* **93**, 1993:1736-1742.

Hamilton, E.L., Geoacoustic Modeling of the Seafloor, *Journal of the Acoustical Society of America*, **68**, 1980:1313-1339.

Holland, C.W., Neumann, P. Sub-bottom scattering: A Modeling Approach, *Journal of the Acoustical Society of America*, **104**, 1998:1363-1373.

Holland, C.W., Hollet, R., Troiano, L. Measurement Technique for bottom scattering in shallow water, *Journal of the Acoustical Society of America*, **108**, 2000:997-1011.

Hodgkiss W.S., Song, H.C. Kuperman, W.A., Akal, T. A long-range and variable focus phase-conjugation experiment in shallow water, *Journal of the Acoustical Society of America*, **105**, 1999:1597s.

Kuperman, W.A., Hodgkiss, W.S., Song, H.C. Phase Conjugation in the Ocean: Experimental demonstration of an acoustic time-reversal mirror, *Journal of the Acoustical Society of America*, **103**, 1998:25-40.

Jackson, D.R. Winebrenner, D.P. Application of the composite roughness model to high frequency bottom backscattering, *Journal of the Acoustical Society of America*, 79, 1410-1422, 1986.

Mackenzie,K.V. Bottom reverberation for 530 and 1030 cps Sound in Deep water, *Journal of the Acoustical Society of America*, **33**, 1961:1498-1504.

Schippers P., ALMOST, An acoustic propagation model, UDT Conference Book of Proceedings, 26 - 28 October 1998, London, UK.

Song, H.C., Kuperman, W.A., Hodgkiss, W.S., Akal, T. Iterative time reversal in the ocean, *Journal of the Acoustical Society of America* **105**, 1999:3176.

Sylva, P., Menard, P., Roy, D. A reconfigurable real-time interpolation beamformer, *IEEE Journal of Oceanic Engineering*, 1986:123-128.

Westwood, E. K., Tindle, C. T., Chapman, N.R. A normal mode model for acoustoelastic ocean.

Annex A
Model for Bottom Scattering

The modelling approach which is fully bi-static is described in Holland and Neumann (1998) where for interface scattering the received level is computed on a horizontal grid. In this paper, the scattering is computed from the water-sediment interface only (although the model can handle scattering from sub-bottom inhomogeneities as well as sub-bottom rough interfaces). The received level for each beam is computed as a sum of delayed, scaled, replicas of the transmit source intensity $S(t)$:

$$RL(t;\theta_m) = 10Log\left[\sum_{k=1}^{2}\sum_{i=1}^{N} S(t-t_i)\, 10^{TL_{i,k}^{in}/10}\, 10^{TL_{i,k}^{out}/10}\, \sigma_k(\theta_{i,k}^{in},\theta_{i,k}^{out})A\right] \qquad \text{A1)}$$

where k is the index for the interface, TL_i^{in} and TL_i^{out} are the transmission losses (including the beam pattern) from the source to scattering cell i and from cell i back to the receiver respectively, σ is the scattering kernel (using the composite roughness theory of Jackson *et al.* (1986) for the water-sediment interface) and A is the area of the cell. For the model used in this study, ray theory was used to compute the TL terms and the grid size was set to 4 m^2. Contributions from the direct blast and the normal incidence air-sea reflection were not included in the calculations. Receiver beampatterns were computed based on an ideal Hanning shaded array.

Annex B
Monitoring the focal point at the seafloor using the DUSS array

An example is provided to show the monitoring of the focal point near the seafloor using the DUSS array. This short array was required because the lowest phone of the VRA was too far (12 m) above the bottom.

Figure 23 shows the time reversed field at the focal point from a 10 ms 3500 Hz CW as measured on the DUSS array. The bottom phone (phone #1) is 1m above the probe source and the other phones are spaced at 2 meter intervals above phone #1. Note that the field decays rapidly with increasing phone number (i.e., above the focal point): an indication that the field is well-focused. Degradation of the focus for successive pings at 10 second intervals is shown in Fig. 24. During this period, some degradation is visible, but the focus remains reasonably pronounced.

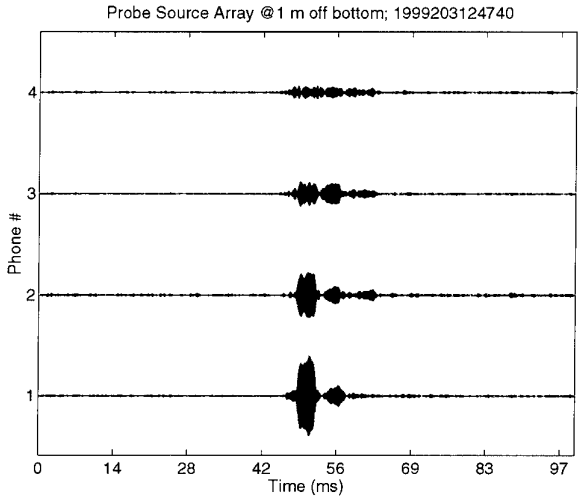

Figure 23 *Time series received on the DUSS array, from a time-reversed signal at Site 2. The probe source was 1 meter above the seafloor. Phone 1 is 1 meter above the probe source and the phones in increasing order are spaced at 2 m above phone #1. The decrease in peak level with increasing distance from phone #1 is an indication of the quality of the focus.*

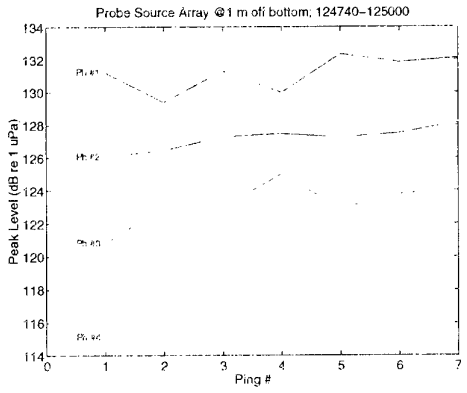

Figure 24 *The time evolution of the focus from a time-reversed ping as observed on the 4 hydrophone array showing a) a good focus at Site 2. Each ping was separated by 10 seconds. The probe source was placed one meter off the bottom.*

[i] The lowest hydrophone on the 4-element array was 1 m above the probe source, and the phones were placed on the same wire as the probe source. The 4-element array was necessary for monitoring the focus when the probe source was placed near the bottom.
[ii] For a source displaced form the boundaries
[iii] 50 ms corresponding to the expected 75 meter SRA MFA offset (see Fig 1).
[iv] The reverberation component of the ALMOST model is not fully coherent and thus does not properly treat the focal region.
[v] This same kind of angular dependence was measured at a site 15 km northwest by Holland et al. (2000) which is believed to have similar sediment properties.
[vi] Despite the high spatial resolution necessary for accurate numerical solution RAM requires only 6sec on a 500Mhz personal computer to propagate out to 3 km.
[vii] There is no formal relationship that we are aware of, linking bandwidth to the vertical resolution. Thus, it is not immediately clear that the modelling results directly correspond to the measurements; however, the observed spot size in the vertical (of order of a few meters) does correspond with the modelled (for the 5 cm vertical resolution) spot size which indicates some degree commensurability.
[viii] It has been assumed that the scattering strength and insonified area are independent of azimuth, i.e., the variability of reverberation in azimuth in Table 3 comes from the bathymetric variability. We have also ignored other (sometimes important) factors inherent in the sonar equation (e.g., it assumes dispersion is negligible and there is no explicit treatment of the angular distribution of incoming/outgoing modes). We would argue that while these assumptions are probably not justified in the general case of reverberation modelling, they are probably adequate for estimating the relative difference in reverberation for various small changes in bottom slope.
[ix] There is a vestige of the null in the NE, E, and SE directions where the relative slope is small.

Document Data Sheet

Security Classification		Project No.
UNCLASSIFIED		04-C
Document Serial No.	**Date of Issue**	**Total Pages**
SR-326	December 2000	40 pp.

Author(s)

Holland, C.W., McDonald, B.E.

Title

Shallow water reverberation from a time reversed mirror

Abstract

Modelling indicates that when the ocean boundaries are the dominant cause of reverberation, the signal-to-reverberation ratio at a target will be increased by generating a time-reversed signal from a vertical array. This occurs because the focusing 1) increases the signal level at the target and 2) reduces the boundary illumination (hence reverberation). An experiment (as part of FAF99) was designed to study the latter (i.e., potential gain against reverberation) resulting from a 3.5 kHz time-reversed signal. Results show the extreme sensitivity of the gain to bathymetric variation and indicate the need for potentially high horizontal spatial resolution in the receive array.

Keywords

Issuing Organization

North Atlantic Treaty Organization
SACLANT Undersea Research Centre
Viale San Bartolomeo 400, 19138 La Spezia, Italy

[From N. America: SACLANTCEN (New York) APO AE 09613]

Tel: +39 0187 527 361
Fax:+39 0187 527 700

E-mail: library@saclantc.nato.int

The SACLANT Undersea Research Centre provides the Supreme Allied Commander Atlantic (SACLANT) with scientific and technical assistance under the terms of its NATO charter, which entered into force on 1 February 1963. Without prejudice to this main task - and under the policy direction of SACLANT - the Centre also renders scientific and technical assistance to the individual NATO nations.

SACLANT Undersea Research Centre
Viale San Bartolomeo 400
19138 San Bartolomeo (SP), Italy

tel: +39 0187 527 (1) or extension
fax: +39 0187 527 700

e-mail: library@saclantc.nato.int

NORTH ATLANTIC TREATY ORGANIZATION